This is a repository copy of *Improving the accuracy of land cover classification in cloud persistent areas using optical and radar satellite image time series*.

White Rose Research Online URL for this paper:
https://eprints.whiterose.ac.uk/156213/

Version: Accepted Version

Methods in Ecology and Evolution

1 ## Improving the accuracy of land cover classification in cloud persistent

2 ## areas using optical and radar satellite image time series

3 Mailys Lopes[1,2,3], Pierre-Louis Frison[3], Merry Crowson[1], Eleanor Warren-Thomas[4], Bambang Hariyadi[5], Winda D.

4 Kartika[5], Fahmuddin Agus[6], Keith C. Hamer[7], Lindsay Stringer[8], Jane K. Hill[4], and Nathalie Pettorelli[1,*]

5 [1]Institute of Zoology, Zoological Society of London, Regent's Park, London NW1 4RY, United Kingdom

6 [2]DYNAFOR, University of Toulouse, INRA, Chemin de Borde Rouge, 31326 Castanet-Tolosan, France

7 [3]LaSTIG, UPEM/IGN, University Paris-Est Marne-la-Vallée, 5 bd Descartes, 77454 Marne-la-Vallée, France

8 [4]Department of Biology, University of York, York YO10 5DD, United Kingdom

9 [5]Biology Education Program, Faculty of Education and Teacher Training, Universitas Jambi, Jl. Raya Jambi-Ma.Bulian km 15

10 Mendalo Darat, Jambi, Indonesia

11 [6]Indonesian Soil Research Institute, Indonesian Center for Agricultural Land Resources Research and Development, Jl. Tentara

12 Pelajar No. 12, Cimanggu, Bogor 16114, Indonesia

13 [7]School of Biology, University of Leeds, Leeds LS2 9JT, United Kingdom

14 [8]School of Earth and Environment, University of Leeds, Leeds LS2 9JT, United Kingdom

15 [*]Correspondence author: Nathalie Pettorelli, Institute of Zoology, Zoological Society of London, Regent's Park, London NW1

16 4RY, United Kingdom, nathalie.petorelli@ioz.ac.uk

17 **Abstract**

18 1. The recent availability of high spatial and temporal resolution optical and radar satellite imagery

19 has dramatically increased opportunities for mapping land cover at fine scales. Fusion of optical and radar

20 images has been found useful in tropical areas affected by cloud cover because of their complementarity.

21 However, the multitemporal dimension these data now offer is often neglected because these areas are

22 primarily characterised by relatively low levels of seasonality and because the consideration of multitemporal

23 data requires more processing time. Hence, land cover mapping in these regions is often based on imagery

24 acquired for a single date or on an average of multiple dates.

25 2. The aim of this work is to assess the added value brought by the temporal dimension of optical

26 and radar time series when mapping land cover in tropical environments. Specifically, we compared the

27 accuracies of classifications based on (i) optical time series, (ii) their temporal average, (iii) radar time

28 series, (iv) their temporal average, (v) a combination of optical and radar time series and (vi) a combination

29 of their temporal averages for mapping land cover in Jambi province, Indonesia, using Sentinel-1 and

30 Sentinel-2 imagery.

31 3. Using the full information contained in the time series resulted in significantly higher classification

32 accuracies than using temporal averages (+14.7% for Sentinel-1, +2.5% for Sentinel-2 and +2% combining

Sentinel-1 and Sentinel-2). Overall, combining Sentinel-2 and Sentinel-1 time series provided the highest accuracies (Kappa = 88.5%).

4. Our study demonstrates that preserving the temporal information provided by satellite image time series can significantly improve land cover classifications in tropical biodiversity hotspots, improving our capacity to monitor ecosystems of high conservation relevance such as peatlands. The proposed method is reproducible, automated, and based on open-source tools satellite imagery.

Key-words: cloud persistent areas, data combination, land cover mapping, remote sensing, satellite image time series, Sentinel-1, Sentinel-2

1 Introduction

Information on land cover and land cover change is key for ecosystem assessment (Cihlar, 2000). Satellite imagery has become indispensable for producing land cover maps over large areas because of its broad spatial coverage. Together with supervised classification approaches, they enable the automatic production of land cover maps. Up until a few years ago, scientists had access to imagery that was either free of charge but collected at coarse to medium spatial resolution (MODIS, Landsat), or at very high spatial resolution (a few meters or less) but costly, limiting land cover mapping to a low level of details or restricted spatial coverage. Since 2014, the availability of free satellite imagery combining both high spatial (10m) and high temporal resolutions through the Copernicus Programme has dramatically changed what can be mapped from space, increasing opportunities to both detect small elements in the landscapes and capture their seasonal variation, thereby enhancing the definition and the classification of vegetation types (Defourny et al., 2019; Gómez, White, & Wulder, 2016; Lambin & Linderman, 2006; Wulder, Hall, Coops, & Franklin, 2004).

Furthermore, the availability of co-registered optical and radar images through Copernicus facilitates the use of fusion for land cover mapping. Image fusion has often been shown to enhance land cover classification accuracy (Clerici, Calderón, & Posada, 2017; Inglada, Vincent, Arias, & Marais-Sicre, 2016; Joshi et al., 2016; Van Tricht, Gobin, Gilliams, & Piccard, 2018) because the information captured by optical and radar sensors is fundamentally different and thus complementary (Kasischke, Melack, & Dobson, 1997). In tropical and boreal areas, optical data availability is often limited by cloud cover leading to radar data being preferred to map land cover in these regions (Asner, 2001; Hoekman, Vissers, & Wielaard, 2010; Kasischke et al., 1997).

Interestingly, the information captured by high temporal resolution sensors has often been neglected in tropical environments, mainly because of the low level of seasonality characterising many of these ecosystems. Therefore, most land cover maps generated for these regions are based on single-date (when cloud-free images are available) or cloud-free composites (see e.g., Crowson et al., 2018; Erinjery, Singh, & Kent, 2018). Cloud-free composites can, however, be difficult and time-consuming to build. Similarly, the multitemporal dimension is often overlooked when combining optical and radar data, mostly because of the unavailability of radar time

series before the launch of Sentinel-1 in 2014 but also because dealing with time series implies more processing time and computing power. Temporal compositing (Griffiths, van der Linden, Kuemmerle, & Hostert, 2013; Vancutsem, Pekel, Bogaert, & Defourny, 2007) of a time series has sometimes been considered to inform land cover mapping, but a large amount of temporal information is lost during this process. Hence, the utility of combining optical and radar satellite image time series for land cover mapping has hardly ever been assessed; known applications include the mapping of agricultural landscapes and the detection of deforestation events (Hirschmugl, Sobe, Deutscher, & Schardt, 2018; Inglada et al., 2016; Kuenzer et al., 2014; Reiche, Verbesselt, Hoekman, & Herold, 2015). To our knowledge, this type of approach has never been considered for mapping land cover in tropical regions of conservation interest with persistent cloud cover and limited level of seasonality. The aim of this study is to fill this gap in knowledge by assessing the added value of preserving the temporal dimension of optical (Sentinel-2) and radar (Sentinel-1) time series. We do so by comparing the outcomes of land cover classifications that consider all the images captured in a given year with classifications using temporal averages. Our work is part of a collaborative UK – Indonesia research project that focused on peatlands in the Jambi province, Indonesia.

Tropical peatlands are very important for carbon storage and are biodiversity hotspots (Wijedasa et al., 2017). Peatland forests have been heavily degraded around the world through deforestation and drainage to make land available for agriculture, leading to carbon release and severe and damaging fires (Miettinen, Shi, & Liew, 2012; Posa, Wijedasa, & Corlett, 2011; Wijedasa et al., 2017). Efforts to restore degraded peatlands – which are part of the Sustainable Development Goals – have recently been made in Indonesia, where most of Southeast Asia's peatlands are located (van Eijk, Leenman, Wibisono, & Giesen, 2009). Accurately monitoring land cover in the humid tropics, such as in the context of restoration efforts in tropical peatlands, is critical to ensure effective conservation and restoration action, and to inform ongoing policies and strategies.

Here we test two hypotheses concerning the accuracy of land cover classification in cloud persistent areas using multitemporal data in the optical and radar domains. As we expect our region of interest to be mainly characterised by a low level of seasonality (although exceptions do exist, e.g. wetlands), the use of all the dates from the optical or radar time series should not significantly improve the accuracy of our land cover map compared to using the temporal average of optical or radar data (H1). Following on from the same principle, the combination of optical and radar time series should have an equivalent classification accuracy to the combination of the temporal averages of the optical and radar images (H2).

2 Materials and Methods

2.1 Study area

The study area is located along the eastern coast of Jambi province in Sumatra (Indonesia, Fig. 1). It covers an area of 12,710 km^2 that is mostly flat. The climate is tropical humid, with an average annual precipitation of 2,400 mm (Hapsari et al., 2017). Even during the dry season (June to September), monthly precipitation is above 100 mm, meaning that the region is primarily subject to a low level of seasonality (Aldrian & Susanto, 2003; Crowson et al., 2018; Karger et al., 2016).

Our study area comprises both anthropogenic environments (agriculture, urban areas) and natural vegetation (peat swamp forest, mineral soil lowland rainforest, mangrove). It is mainly dominated by plantations (oil palm, coconut palm, areca palm, acacia, rubber) that have replaced forests as large monoculture or smallholder plantations. The eastern part of the study area is dominated by Berbak National Park (about 1,850 km^2), which is a protected (IUCN category II), undrained peat swamp forest that supports a large amount of biodiversity (Giesen, 2004). The forest is surrounded by fern-dominated scrublands which are regrowth areas left unmanaged after severe fires. The Sungai Buloh Forest Reserve is located in the central part of the study area and covers an area of about 120 km^2. Mangroves are primarily found along the coast.

2.2 Reference data

Reference data were generated through visual interpretation of very high spatial resolution images (2017 Google Earth imagery and 2017 PlanetScope scenes) using prior knowledge of the region acquired during field visits. These reference data were generated in an opportunistic way but ensuring a good spatial distribution of the polygons over the whole study area (Fig. 1). We primarily used the same classes as Crowson et al. (2018), namely peat swamp forest, water, urban, palm trees (all combined), acacia trees, fern/scrublands, bare ground; only a mangrove class was added to this original list. Mangrove polygons were digitized using the USGS Global distribution of mangroves (`http://data.unep-wcmc.org/datasets/4`). In total, reference data comprised 1399 polygons distributed in 8 classes (Table 1), following approximately the proportion of area covered by each class over the study area, representing about 1.5 millions pixels (1.2% of the study area).

2.3 Satellite imagery

2.3.1 Sentinel-2

We used optical images acquired by Sentinel-2 along two different orbit paths to cover the whole study area (7 tiles in total). We downloaded all the images acquired in 2017 presenting a maximum of 70% cloud cover ; this resulted in 10 to 12 dates per tile. The Level L1C images (orthorectified and radiometrically corrected to

Top of Atmosphere reflectance) were processed to Level L2A surface reflectances (corrected for atmospheric effects and slope effects) using the Sen2Cor processor (version 2.5.5) (`http://step.esa.int/main/third-party-plugins-2/sen2cor/sen2cor_v2-5-5/`). The algorithm provides a scene classification including pixels affected by noise such as clouds and cloud shadows. Those pixels were masked and filled using a temporal gap-filling method (*Image Time Series Gap Filling* application from the Orfeo ToolBox (version 6.6); OTB (Grizonnet et al., 2017; OTB Development Team, 2018)) that replaces the masked/invalid pixels with a value interpolated from the valid dates of the time series. During this process, the time series of each tile were also resampled to the same temporal grid to facilitate the subsequent mosaicking. The temporal grid was chosen based on the original 10 temporal acquisitions of the main (central) tile of the study area. In the end, all the pixels of the study area had the same dates: 2017-02-20, 2017-03-12, 2017-07-10, 2017-07-25, 2017-07-30, 2017-08-19, 2017-10-08, 2017-10-18, 2017-11-22, 2017-12-22. This temporal gap-filling process was done for each of the ten Sentinel-2 spectral bands at spatial resolutions of 10m and 20m (resampled to 10m resolution using a nearest neighbour interpolation). Finally, the tiles from the two orbits were mosaicked using a mosaic technique from the OTB application (`https://github.com/remicres/otb-mosaic`) that blends all the images on the overlapping areas, resulting in a seamless unique raster covering the whole study area.

2.3.2 Sentinel-1

Since radar images are not affected by cloud cover, all the Sentinel-1 images acquired between February and December 2017 over the study area were used to match the temporal coverage of the optical time series. In total, there were 26 images, acquired every 12 days from 2017-02-03 to 2017-12-24. The images were acquired over the same orbit, so no mosaicking was required. The Level-1 Ground Range Detected High Resolution (GRDH) were radiometrically calibrated to the radar backscattering coefficient σ^0 for both polarizations VV and VH using OTB application *SAR Radiometric Calibration* (Laur et al., 2004). They were then orthorectified to correct for the geometric distortions using the OTB application *OrthoRectification* (Small & Schubert, 2008). The output spatial resolution was 10m per pixel. The images were subsequently converted from intensity to the logarithm dB scale, and the ratio VH/VV was computed as a third polarization.

Radar data are affected by speckle effects that are often filtered for land cover mapping applications. When using single date images, a spatial filtering is usually done, at the cost of degrading the spatial resolution. When using multitemporal images, a temporal filter such as the Quegan filter (Quegan & Yu, 2001) reduces the speckle effects without affecting much the spatial resolution (Trouvé, Chambenoit, Classeau, & Bolon, 2003). Simply computing the temporal average has the advantage of drastically reducing the speckle effects (Zhao et al., 2019) without degrading the spatial resolution, but obviously at the cost of the temporal information. In this study, we thus applied the Quegan filter on the time series to exploit the temporal information and

computed the temporal average from the unfiltered images.

2.4 Classification protocol

The classification was performed using Random Forest (RF), one of the fastest algorithms for pixel-based classification with a large number of pixels and variables (Breiman, 2001; Pelletier, Valero, Inglada, Champion, & Dedieu, 2016). We used RF implemented in OTB applications with the following parameters: maximum depth of tree = 25; minimum number of samples in each node = 25; maximum number of trees in the forest = 100, chosen following Pelletier et al. (2016) recommendations, as a good compromise between classification accuracy and computation time. Pelletier et al. (2016) have shown that the RF parameters have little influence on the performance of the classification. The reference dataset was split randomly but in a stratified fashion into disjoint training (75%) and validating (25%) subsets, preserving the initial proportions of each class in the two subsets. The split was performed at the polygon level in order to ensure an independent set of pixels between the training and the validation steps (i.e., no pixels belonging to the same polygon in the training and validating subsets). The resulting classification maps were sieved to eliminate isolated pixels and thus to reduce the 'salt and pepper' effect associated with a pixel-based classification. Finally, the accuracy of the produced land cover maps was assessed by computing the confusion matrix based on the validation subset and by extracting accuracy metrics (Kappa coefficient, User's accuracy, Producer's accuracy). The training and validation data are issued from the same dataset (but different polygons). As such, the resulting accuracies might be slightly overestimated as they are not totally independent (Olofsson, Foody, Stehman, & Woodcock, 2013). However, this is not an issue here as the objective of this paper is to compare the performances of different types of inputs, produced from the same set of training and validation pixels.

Six land cover classifications based on six different inputs were tested and compared:

- $S1_a$: annual temporal average of Sentinel-1 images in the 3 polarizations,

- $S1_t$: Sentinel-1 time series in the 3 polarizations,

- $S2_a$: annual temporal average of Sentinel-2 in the 10 spectral bands,

- $S2_t$: Sentinel-2 time series in the 10 spectral bands,

- $S1_a + S2_a$: the combination of Sentinel-1 and Sentinel-2 annual temporal averages,

- $S1_t + S2_t$: the combination of Sentinel-1 and Sentinel-2 time series.

For the latter two, the combination was performed by stacking both annual temporal averages / time series prior to classification.

Additionally, an *a posteriori* fusion of classifications based on Sentinel-2 and Sentinel-1 was performed to account for undetected clouds by the cloud-masking algorithm. We therefore added a supplementary "cloud"

class to the classifications based on Sentinel-2 data (by adding non-detected cloud polygons in the training dataset), so that areas of permanent non-detected cloud cover could be identified. Then, the pixels tagged as "clouds" in the subsequent classification were replaced with the results of the classification obtained with Sentinel-1. The outcomes of this *a posteriori* classification are only presented for the $S1_t + S2_t$ classification (named "$S1_t + S2_t$ fused $S1_t$").

Kappa coefficients associated with each pair of confusion matrices were compared to identify possible significant differences in accuracies associated with our six land cover classifications (Congalton & Green, 1998). The test statistic Z was assessed as follows:

$$Z = \frac{|K_1 - K_2|}{\sqrt{\sigma_1^2 + \sigma_2^2}}$$

where K_i is the Kappa coefficient resulting from the ith confusion matrix and σ_i is the large sample variance of K_i (see Congalton & Green, 1998).

The workflow of the preprocessing of the images and of the classification process can be found in Fig. 2.

3   Results

Contrary to our first expectation (H1), using the optical or radar time series resulted in significantly (*P*-value < 0.001) higher Kappa coefficient than using their temporal average counterparts (82.9% for $S1_t$ against 68.2% for $S1_a$ and 79.0% for $S2_t$ against 76.5% for $S2_a$). Similarly, using the combination of optical and radar time series improved significantly (*P*-value < 0.001) the land cover classification compared to using the combination of optical and radar temporal averages (from Kappa = 86.6% for $S1_a + S2_a$ to Kappa = 88.5% for $S1_t + S2_t$), contradicting our second hypothesis (H2).

In terms of per-class accuracies (see Table in the Supporting Information), most of the classes benefit from the use of the time series, especially palm trees, fern, and mangrove. Most classes reached their highest accuracies when combining Sentinel-2 and Sentinel-1 time series. Mangroves were not well identified using Sentinel-1 compared to Sentinel-2.

In terms of land cover maps, the maps based on the time series look visually better (less noisy) than the ones based on temporal averages (Fig. 3). Maps based on Sentinel-1 data only are riddled with 'salt and pepper' noise, resulting in many misclassified pixels among classes such as forest and palm plantations. In addition, Sentinel-1 data tend to confuse palm trees, mangroves and peat swamp forest (Fig. 3, top). Sentinel-2 based classifications look more realistic but show big "holes" in the classes due to the presence of undetected clouds, often classified as palm plantations or urban area (Fig. 3, middle). The combination of Sentinel-1 and Sentinel-2 time series lead to visually better maps (Fig. 3, bottom), especially when fusing

218    $S1_t + S2_t$ with $S1_t$ (Fig. 4, bottom).

219   Overall, the best classification accuracy was obtained when replacing pixels identified as clouds by the
220 classifier using $S1_t + S2_t$ (Fig. 4, top) with results from $S1_t$ classification: the Kappa coefficient reached
221 89.4% ($S1_t + S2_t$ fused $S1_t$, Fig. 4, bottom), significantly (P-value < 0.001) improving by 1% the accuracy
222 of the $S1_t + S2_t$ classification.

4   Discussion

224 Our results provide for the first time a measure of the level of accuracy gained when using all the temporal
225 information of optical and radar satellite image time series to map land cover in large areas of conservation
226 value with persistent cloud cover. Despite the relatively low level of seasonality characterising most of
227 the habitats found in these landscapes, using time series significantly improved the discrimination between
228 vegetation classes compared to using annual temporal averages, suggesting that seasonal differences occur
229 among classes and should not be neglected. Combining optical and radar time series also significantly
230 improved our land cover classification, with radar data nicely complementing optical data in clouded areas.
231 Our results support the conclusions of Hirschmugl et al. (2018) who reported improved accuracy in the
232 detection of deforestation events in Malawi using time series of Sentinel-2 and/or Sentinel-1 data compared to
233 monotemporal data. Steinhausen, Wagner, Narasimhan, and Waske (2018) also found an improved accuracy
234 of land cover mapping in monsoon regions in India when increasing the number of Sentinel-1 scenes to one
235 Sentinel-2 scene, but Mercier et al. (2019) found little improvement when adding Sentinel-1 time series to
236 the one Sentinel-2 scene considered for mapping land cover in a forest-agriculture mosaic in Brazil. For these
237 two last studies, however, the use of Sentinel-2 time series was not attempted due to heavy cloud cover.

238   To our surprise, the accuracy of the classification based on radar time series was 4% higher than the
239 classification based on optical time series. More accurate classifications do not systematically generate,
240 however, "better" maps. First, maps derived from radar data are riddled with noise due to the speckle
241 effect that is typically associated with radar imagery; although filtered, this effect was still present in our
242 classification and led to numerous misclassified pixels. An additional filter could be applied to reduce this
243 effect, but it would be at the cost of spatial resolution, losing details such as drainage channels. Second,
244 and perhaps surprisingly, mangroves were not well identified using Sentinel-1, being often confused with
245 peat swamp forest. The main difference between mangroves and peat swamp forest is that mangroves are
246 submerged by sea water all year long (Wikramanayake, Dinerstein, Loucks, & Pimm, 2002). Radar data are
247 sensitive to soil wetness and were therefore expected to capture this difference well (Kasischke et al., 1997);
248 the issue here, however, is that canopy cover is very dense, meaning that Sentinel-1 C-band might not have
249 been able to penetrate it. Li, Lu, Moran, Dutra, and Batistella (2012) found that L-band provides much

better accuracy than C-band for land cover mapping in tropical moist regions. However, neither of them could separate the types of forests investigated, showing the unsuitability of radar data alone to accurately map the very similar vegetation classes found in their study area. In our study, Sentinel-2 was much better at discriminating between mangrove and peat swamp forest than Sentinel-1.

The use of optical data in regions affected by persistent cloud cover, even as part of the fusion of optical and radar data, nevertheless raises technical issues. When areas particularly affected by cloud cover are detected, they can be automatically masked and complemented by radar data. In our case, however, many clouds were not detected by our chosen cloud detector algorithm, which caused important problems in the classification process. Specifically, the training of the classifier was made on a dataset that included "cloudy" Sentinel-2 pixels associated with various land cover categories, which ultimately reduced separability between classes. When looking at the generated land cover map, it resulted in holes in the land covers, as described in the results section. To overcome this issue, we had to add a supplementary class "clouds" in the classification involving Sentinel-2 data to identify these rogue areas. Although requiring additional steps in our overall classification process (Fig. 2), this approach allowed us to better detect clouds and produced the most accurate land cover map (Fig. 4, bottom).

The proposed method can easily be applied to large areas and reproduced in other regions because it is based on freely-accessible satellite imagery and all the steps can be processed automatically in a processing chain reliant on open-source software tools. Unlike previous attempts to map peat land cover in the region creating a manual cloud-free composite (see e.g., Crowson et al., 2018), no manual inputs are required (except to form the reference dataset, including persistent cloud cover polygons, but this step is essential to all supervised classifications) ; the proposed method is thus time-saving and less sensitive to human errors.

Altogether, this work demonstrates how the combination of recent algorithmic advances in big data processing and new earth observation capabilities associated with the development of the Copernicus programme has the potential to significantly improve our ability to monitor key ecosystems in remote regions. Combining optical and radar time series indeed resulted in higher accuracies for the mapping of peat swamp forests, allowing environmental managers and policy makers to access up-to-date, fine scale information about peatland distribution, thereby supporting efforts to protect and restore these ecosystems. Combining optical and radar time series to map land cover can seem daunting to ecologists used to classifying single optical images; however, recent computational advances as well as existing spatial compatibilities between Sentinel-1 and Sentinel-2 imagery significantly improve the accessibility of such approaches, and our work clearly demonstrates that efforts to go beyond classical approaches do pay off. We therefore urge scientists and practitioners to start exploiting the full capacity of Sentinel-2 and Sentinel-1 to monitor sensitive habitats in areas of conservation interest.

9

Acknowledgements

Authors' contributions

ML, PLF and NP conceived the ideas and designed the methodology; BH, WDK, MC and EWT collected the reference data with the help of FA; ML performed the image processing and the analysis; ML and NP wrote the manuscript with feedback from PLF, MC, EWT, JKH, FA, KCH and LS. All authors contributed critically to the drafts and gave final approval for publication.

Data Availability

The satellite images used in this study can be downloaded in the Copernicus Open Access Hub (`https://scihub.copernicus.eu/dhus/`). For Sentinel-2, the following search parameters were used: Sensing period: 2017-01-01 to 2017-12-31, Mission: Sentinel-2, Product Type: S2MSI2A, Relative Orbit Number: 118 or 75, Cloud Cover %: 0 TO 70. For Sentinel-1, the following search parameters were used: Sensing period: 2017-02-01 to 2017-12-31, Mission: Sentinel-1, Product Type: GRD, Sensor Mode: IW, Relative Orbit Number: 171. A polygon encompassing the study area (Fig. 1) was drawn manually on the search platform. The images were processed using version 6.6 (doi: 10.5281/zenodo.1294917) of the Orfeo ToolBox open-source software available at `https://doi.org/10.5281/zenodo.1294916` (OTB Development Team, 2018). The latest version of the Orfeo Toolbox can be downloaded at `https://www.orfeo-toolbox.org`.

References

Aldrian, E., & Susanto, R. D. (2003). Identification of three dominant rainfall regions within Indonesia and their relationship to sea surface temperature. *International Journal of Climatology*, *23*(12), 1435-1452. doi: 10.1002/joc.950

Asner, G. P. (2001). Cloud cover in Landsat observations of the Brazilian Amazon. *International Journal of Remote Sensing*, *22*(18), 3855-3862. doi: 10.1080/01431160010006926

Breiman, L. (2001). Random forests. *Machine Learning*, *45*(1), 5–32.

Cihlar, J. (2000). Land cover mapping of large areas from satellites: Status and research priorities. *International Journal of Remote Sensing*, *21*(6-7), 1093-1114. doi: 10.1080/014311600210092

Clerici, N., Calderón, C. A. V., & Posada, J. M. (2017). Fusion of Sentinel-1A and Sentinel-2A data for land cover mapping: a case study in the lower Magdalena region, Colombia. *Journal of Maps*, *13*(2), 718-726. doi: 10.1080/17445647.2017.1372316

Congalton, R., & Green, K. (1998). *Assessing the accuracy of remotely sensed data: Principles and practices*. CRC-Press.

Crowson, M., Warren-Thomas, E., Hill, J. K., Hariyadi, B., Agus, F., Saad, A., . . . Pettorelli, N. (2018). A comparison of satellite remote sensing data fusion methods to map peat swamp forest loss in Sumatra, Indonesia. *Remote Sensing in Ecology and Conservation*. doi: 10.1002/rse2.102

Defourny, P., Bontemps, S., Bellemans, N., Cara, C., Dedieu, G., Guzzonato, E., . . . Koetz, B. (2019). Near real-time agriculture monitoring at national scale at parcel resolution: Performance assessment of the Sen2-Agri automated system in various cropping systems around the world. *Remote Sensing of Environment*, *221*, 551 - 568. doi: https://doi.org/10.1016/j.rse.2018.11.007

Erinjery, J. J., Singh, M., & Kent, R. (2018). Mapping and assessment of vegetation types in the tropical rainforests of the Western Ghats using multispectral Sentinel-2 and SAR Sentinel-1 satellite imagery. *Remote Sensing of Environment*, *216*, 345 - 354. doi: https://doi.org/10.1016/j.rse.2018.07.006

Giesen, W. (2004). *Causes of peat swamp forest degradation in Berbak NP, Indonesia, and recommendations for restoration* (Tech. Rep.). ARCADIS Euroconsult. doi: 10.13140/RG.2.2.16544.64006

Griffiths, P., van der Linden, S., Kuemmerle, T., & Hostert, P. (2013, Oct). A pixel-based Landsat compositing algorithm for large area land cover mapping. *IEEE Journal of Selected Topics in Applied Earth Observations and Remote Sensing*, *6*(5), 2088-2101. doi: 10.1109/JSTARS.2012.2228167

Grizonnet, M., Michel, J., Poughon, V., Inglada, J., Savinaud, M., & Cresson, R. (2017). Orfeo ToolBox: open source processing of remote sensing images. *Open Geospatial Data, Software and Standards*, *2*(1), 15. doi: 10.1186/s40965-017-0031-6

Gómez, C., White, J. C., & Wulder, M. A. (2016). Optical remotely sensed time series data for land cover

classification: A review. *ISPRS Journal of Photogrammetry and Remote Sensing*, *116*, 55 - 72. doi: https://doi.org/10.1016/j.isprsjprs.2016.03.008

Hapsari, K. A., Biagioni, S., Jennerjahn, T. C., Reimer, P. M., Saad, A., Achnopha, Y., ... Behling, H. (2017). Environmental dynamics and carbon accumulation rate of a tropical peatland in Central Sumatra, Indonesia. *Quaternary Science Reviews*, *169*, 173 - 187. doi: https://doi.org/10.1016/j.quascirev.2017.05.026

Hirschmugl, M., Sobe, C., Deutscher, J., & Schardt, M. (2018). Combined use of optical and synthetic aperture radar data for REDD+ applications in Malawi. *Land*, *7*(4). doi: 10.3390/land7040116

Hoekman, D. H., Vissers, M. A. M., & Wielaard, N. (2010). PALSAR wide-area mapping of Borneo: Methodology and map validation. *IEEE Journal of Selected Topics in Applied Earth Observations and Remote Sensing*, *3*(4), 605-617. doi: 10.1109/JSTARS.2010.2070059

Inglada, J., Vincent, A., Arias, M., & Marais-Sicre, C. (2016). Improved Early Crop Type Identification By Joint Use of High Temporal Resolution SAR And Optical Image Time Series. *Remote Sensing*, *8*(5). Retrieved from `https://www.mdpi.com/2072-4292/8/5/362` doi: 10.3390/rs8050362

Joshi, N., Baumann, M., Ehammer, A., Fensholt, R., Grogan, K., Hostert, P., ... Waske, B. (2016). A review of the application of optical and radar remote sensing data fusion to land use mapping and monitoring. *Remote Sensing*, *8*(1).

Karger, D. N., Conrad, O., Böhner, J., Kawohl, T., Kreft, H., Soria-Auza, R. W., ... Kessler, M. (2016). *CHELSA climatologies at high resolution for the earth's land surface areas (Version 1.1)*. World Data Center for Climate (WDCC) at DKRZ. doi: 10.1594/WDCC/CHELSA_v1_1

Kasischke, E. S., Melack, J. M., & Dobson, M. C. (1997). The use of imaging radars for ecological applications—a review. *Remote Sensing of Environment*, *59*(2), 141 - 156. doi: https://doi.org/10.1016/S0034-4257(96)00148-4

Kuenzer, C., Ottinger, M., Wegmann, M., Guo, H., Wang, C., Zhang, J., ... Wikelski, M. (2014). Earth observation satellite sensors for biodiversity monitoring: potentials and bottlenecks. *International Journal of Remote Sensing*, *35*(18), 6599-6647. doi: 10.1080/01431161.2014.964349

Lambin, E. F., & Linderman, M. (2006). Time series of remote sensing data for land change science. *IEEE Transactions on Geoscience and Remote Sensing*, *44*(7), 1926-1928. doi: 10.1109/TGRS.2006.872932

Laur, H., Bally, P., Meadows, P., Sanchez, J., Schaettler, B., Lopinto, E., & Esteban, D. (2004). *Derivation of the backscattering coefficient σo in ESA ERS SAR PRI products* (Calibration/Validation Document Nos. Issue 2, Rev. 5f). ESA.

Li, G., Lu, D., Moran, E., Dutra, L., & Batistella, M. (2012). A comparative analysis of ALOS PALSAR L-band and RADARSAT-2 C-band data for land-cover classification in a tropical moist region. *ISPRS Journal of Photogrammetry and Remote Sensing*, *70*, 26 - 38. doi: https://doi.org/10.1016/j.isprsjprs

371   .2012.03.010

372 Mercier, A., Betbeder, J., Rumiano, F., Baudry, J., Gond, V., Blanc, L., . . . Hubert-Moy, L. (2019).

373   Evaluation of Sentinel-1 and 2 time series for land cover classification of forest–agriculture mosaics in

374   temperate and tropical landscapes. *Remote Sensing*, *11*(8). doi: 10.3390/rs11080979

375 Miettinen, J., Shi, C., & Liew, S. C. (2012). Two decades of destruction in Southeast Asia's peat swamp

376   forests. *Frontiers in Ecology and the Environment*, *10*(3), 124-128. doi: 10.1890/100236

377 Olofsson, P., Foody, G. M., Stehman, S. V., & Woodcock, C. E. (2013). Making better use of accuracy

378   data in land change studies: Estimating accuracy and area and quantifying uncertainty using stratified

379   estimation. *Remote Sensing of Environment*, *129*, 122 - 131. doi: https://doi.org/10.1016/j.rse.2012

380   .10.031

381 OTB Development Team. (2018, June 21). *Orfeo toolbox 6.6.0.* Zenodo. doi: 10.5281/zenodo.1294917

382 Pelletier, C., Valero, S., Inglada, J., Champion, N., & Dedieu, G. (2016). Assessing the robustness of random

383   forests to map land cover with high resolution satellite image time series over large areas. *Remote*

384   *Sensing of Environment*, *187*, 156 - 168. doi: https://doi.org/10.1016/j.rse.2016.10.010

385 Posa, M. R. C., Wijedasa, L. S., & Corlett, R. T. (2011). Biodiversity and Conservation of Tropical Peat

386   Swamp Forests. *BioScience*, *61*(1), 49-57. doi: 10.1525/bio.2011.61.1.10

387 Quegan, S., & Yu, J. J. (2001). Filtering of multichannel SAR images. *IEEE Transactions on Geoscience and*

388   *Remote Sensing*, *39*(11), 2373-2379. doi: 10.1109/36.964973

389 Reiche, J., Verbesselt, J., Hoekman, D., & Herold, M. (2015). Fusing Landsat and SAR time series to detect

390   deforestation in the tropics. *Remote Sensing of Environment*, *156*, 276 - 293. doi: https://doi.org/

391   10.1016/j.rse.2014.10.001

392 Small, D., & Schubert, A. (2008). Guide to ASAR geocoding. *ESA-ESRIN Technical Note RSL-ASAR-GC-*

393   *AD*, *1*.

394 Steinhausen, M. J., Wagner, P. D., Narasimhan, B., & Waske, B. (2018). Combining Sentinel-1 and Sentinel-2

395   data for improved land use and land cover mapping of monsoon regions. *International Journal of Applied*

396   *Earth Observation and Geoinformation*, *73*, 595 - 604. doi: https://doi.org/10.1016/j.jag.2018.08.011

397 Trouvé, E., Chambenoit, Y., Classeau, N., & Bolon, P. (2003). Statistical and operational performance as-

398   sessment of multitemporal SAR image filtering. *IEEE Transactions on Geoscience and Remote Sensing*,

399   *41*(11), 2519-2530. doi: 10.1109/TGRS.2003.817270

400 Vancutsem, C., Pekel, J., Bogaert, P., & Defourny, P. (2007). Mean compositing, an alternative strategy

401   for producing temporal syntheses. concepts and performance assessment for SPOT VEGETATION time

402   series. *International Journal of Remote Sensing*, *28*(22), 5123-5141. doi: 10.1080/01431160701253212

403 van Eijk, P., Leenman, P., Wibisono, I. T., & Giesen, W. (2009). Regeneration and restoration of degraded

404   peat swamp forest in Berbak NP, Jambi, Sumatra, Indonesia. *Malayan Nature Journal*, *61*, 223-241.

Van Tricht, K., Gobin, A., Gilliams, S., & Piccard, I. (2018). Synergistic Use of Radar Sentinel-1 and Optical Sentinel-2 Imagery for Crop Mapping: A Case Study for Belgium. *Remote Sensing*, *10*(10). doi: 10.3390/rs10101642

Wijedasa, L. S., Jauhiainen, J., Könönen, M., Lampela, M., Vasander, H., Leblanc, M.-C., ... Andersen, R. (2017). Denial of long-term issues with agriculture on tropical peatlands will have devastating consequences. *Global Change Biology*, *23*(3), 977-982. doi: 10.1111/gcb.13516

Wikramanayake, E., Dinerstein, E., Loucks, C., & Pimm, S. (2002). *Terrestrial ecoregions of the indo-pacific: A conservation assessment*. Island Press.

Wulder, M. A., Hall, R. J., Coops, N. C., & Franklin, S. E. (2004). High Spatial Resolution Remotely Sensed Data for Ecosystem Characterization. *BioScience*, *54*(6), 511-521. doi: 10.1641/0006-3568(2004) 054[0511:HSRRSD]2.0.CO;2

Zhao, W., Deledalle, C., Denis, L., Maître, H., Nicolas, J., & Tupin, F. (2019, June). Ratio-based multi-temporal SAR images denoising: RABASAR. *IEEE Transactions on Geoscience and Remote Sensing*, *57*(6), 3552-3565. doi: 10.1109/TGRS.2018.2885683

Tables

Table 1: Classes used in this study (see Crowson et al. (2018) for a description of the classes).

Class	Number of reference polygons	pixels
Peat swamp forest	173	353,241
Water	207	139,713
Urban	164	13,549
Palm trees	250	211,082
Acacia trees	212	360,331
Fern/scrublands	165	171,271
Bare ground	147	116,423
Mangrove	81	131,177
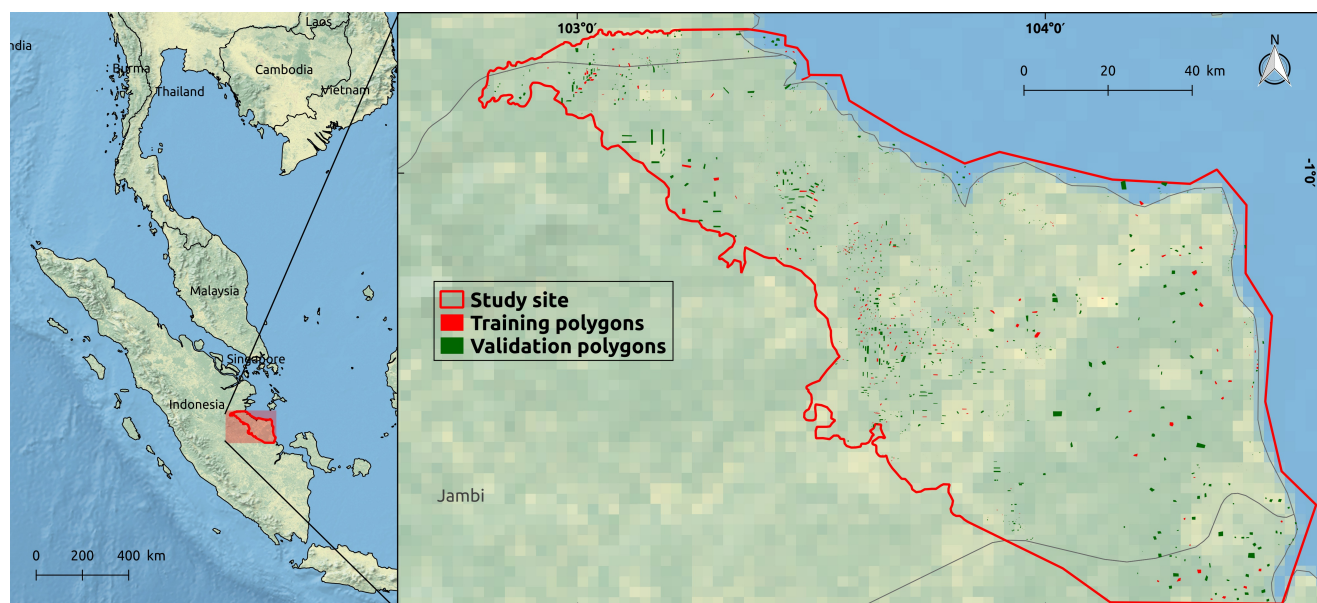
Figures

Figure 1: Location of the study area (red lines) in Jambi province, Sumatra (Indonesia) and of the reference polygons. Data: Natural Earth (`https://www.naturalearthdata.com`).
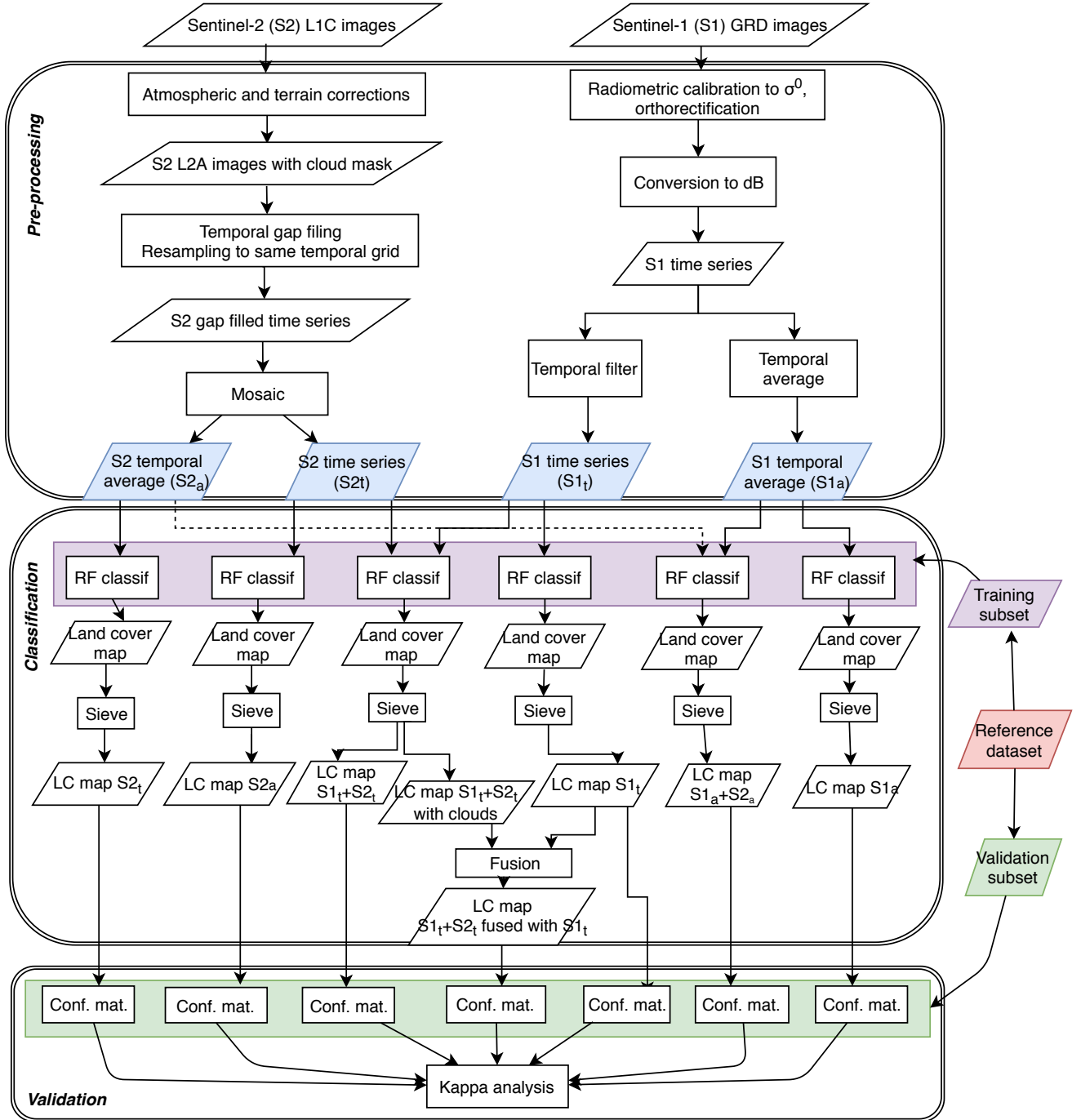
Figure 2: Workflow of the processing and the classification processes. RF classif.: Random Forest classification, LC: land cover, Conf. mat: confusion matrix.
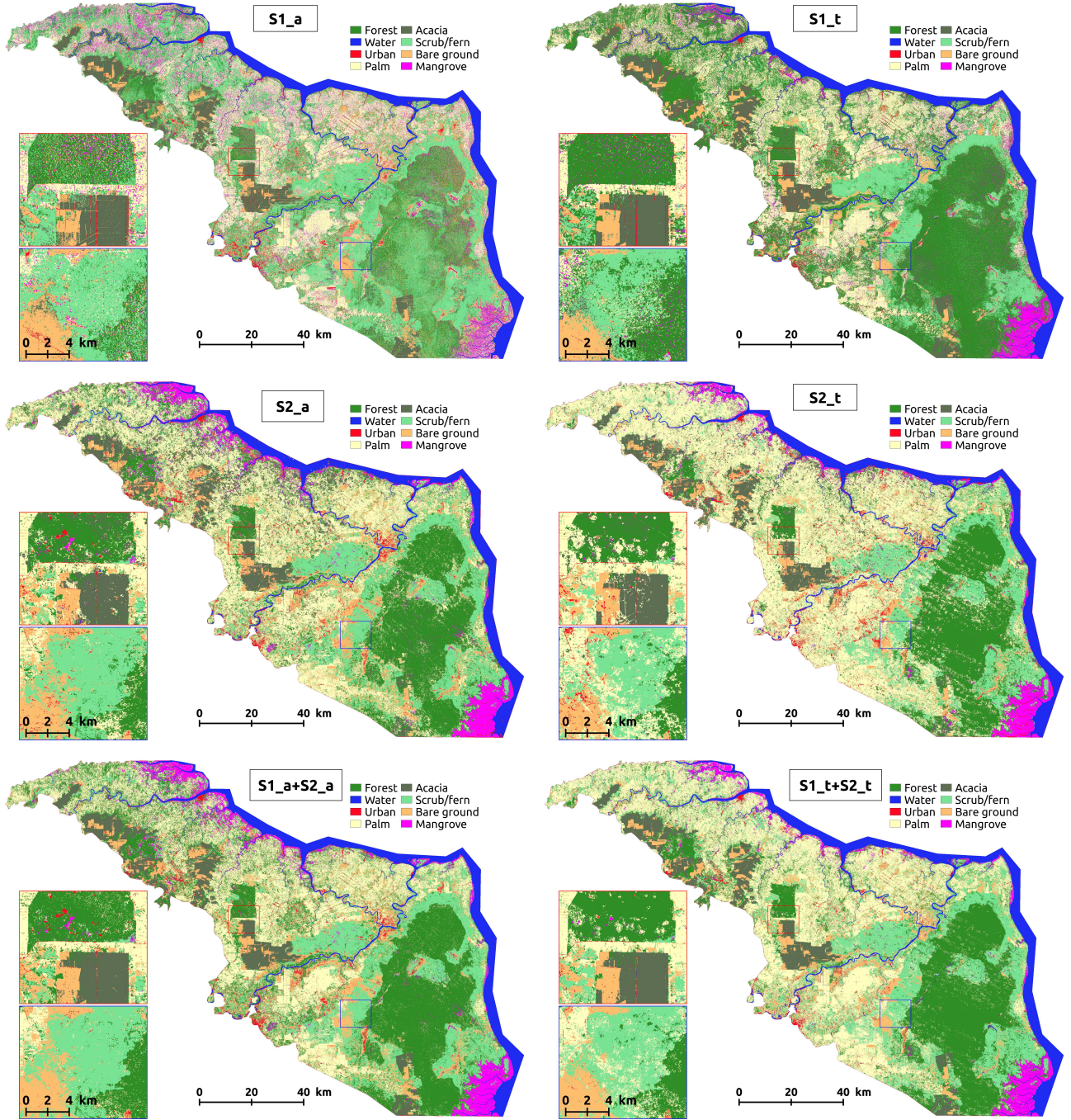
Figure 3: Land cover maps produced from Sentinel-1 (S1$_a$ (average): Kappa = 68.2%, S1$_t$ (time series): Kappa = 82.9%, top), Sentinel-2 (S2$_a$ (average): Kappa = 76.5%, S2$_t$ (time series): Kappa = 79.0%,middle) and combination of both (S1$_a$+S2$_a$: Kappa = 86.6%, S1$_t$+S2$_t$: Kappa = 88.5%, bottom).
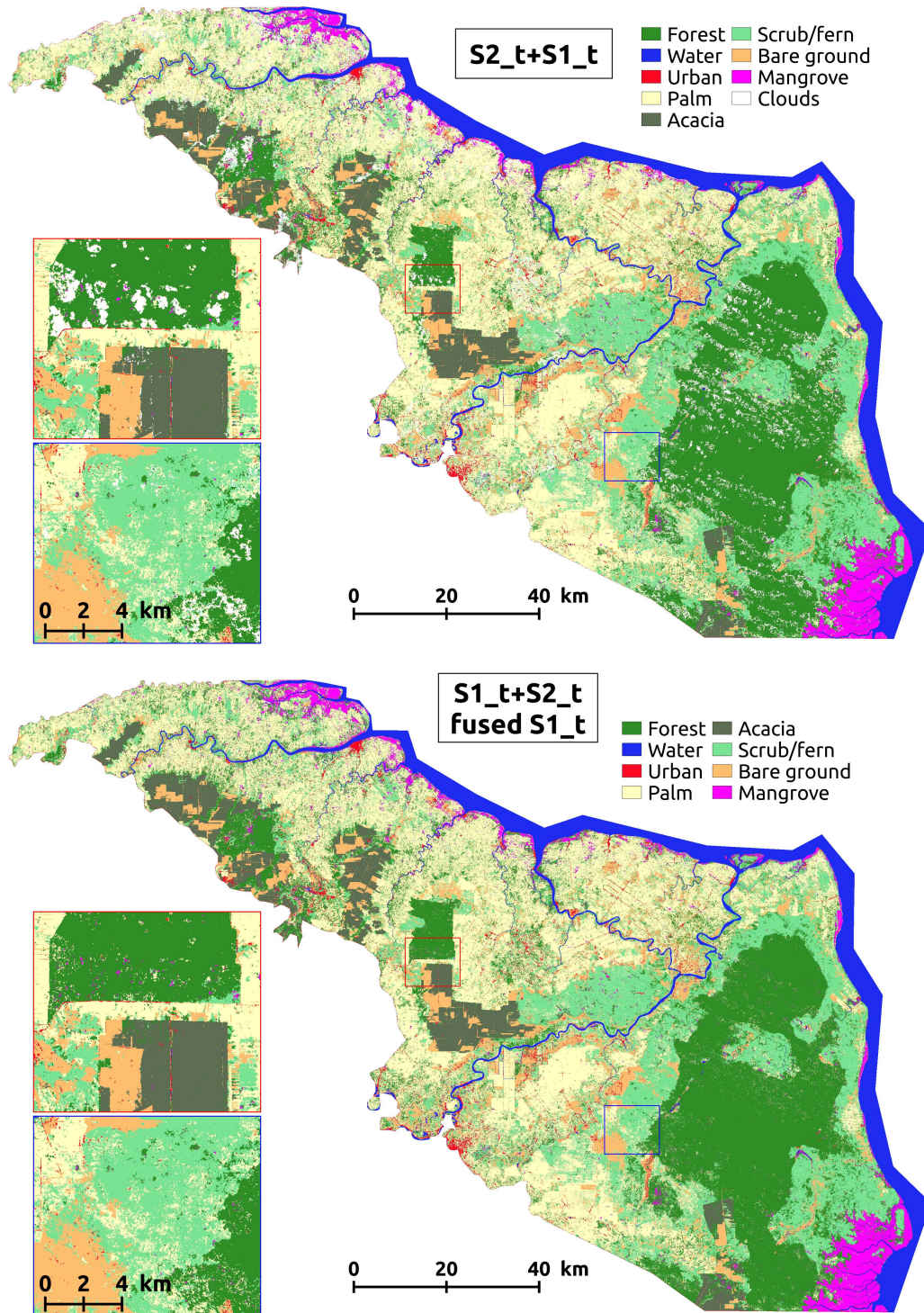
Figure 4: Land cover maps produced from Sentinel-1 & Sentinel-2 time series with cloud class (top) and clouds replaced with Sentinel-1 ($S1_t$) classification ($S1_t$+$S2_t$ fused $S1_t$),Kappa = 89.4, bottom).